

The regulatory mechanism of the caspase 6 pro-domain revealed by crystal structure and biochemical assays

Qin Cao, Xiao-Jun Wang,
Lan-Fen Li and Xiao-Dong Su*

State Key Laboratory of Protein and Plant Gene Research, and Biodynamic Optical Imaging Center (BIOPIC), School of Life Sciences, Peking University, Beijing 100871, People's Republic of China

Correspondence e-mail: xdsu@pku.edu.cn

Caspase 6 (CASP6) is a neuron degeneration-related protease and is widely considered to be a potential drug-design target against neurodegenerative diseases such as Huntington's disease and Alzheimer's disease. The N-terminal pro-peptide of CASP6, also referred to as the pro-domain, contains 23 residues and its functional role remains elusive. In this study, the crystal structure of a full-length CASP6 zymogen mutant, proCASP6H121A, was solved. Although the pro-domain was flexible in the crystal, without visible electron density, structural analyses combined with biochemical assays revealed that the pro-domain inhibited CASP6 auto-activation by inhibiting intramolecular cleavage at the intersubunit cleavage site TEVD¹⁹³ and also by preventing this site from intermolecular cleavage at low protein concentration through a so-called 'suicide-protection' mechanism. Further experiments showed that the length of the pro-domain and the side chain of Asn18 played critical roles in suicide protection. These results disclosed a new inhibitory mechanism of CASP6 and shed light on the pathogenesis and therapeutically relevant study of CASP6-related neurodegenerative diseases.

Received 14 June 2013
Accepted 29 August 2013

PDB Reference:
proCASP6H121A, 4iyr

1. Introduction

Caspases are a family of cysteine proteases which are the major executors of apoptosis and inflammation. Caspases can be divided into three groups (inflammatory caspases, apoptotic initiators and effectors) based on their function and sequence similarities; CASP6 is classified as an effector caspase together with CASP3 and CASP7 (Yan & Shi, 2005; Pop & Salvesen, 2009). The three effector caspases are expressed as dimeric zymogens and each monomer contains a short pro-domain, a large subunit (p20), an intersubunit linker (L) and a small subunit (p10). The canonical activation process of effector caspases involves proteolysis at the cleavage sites between the pro-domain, p20 and p10 by initiator caspases (CASP8 and CASP9) to form active enzymes (Boatright & Salvesen, 2003). However, in contrast to the above scheme, CASP6 is often activated by CASP3 rather than initiator caspases (Slee *et al.*, 1999; Simon *et al.*, 2012) and it can also undergo auto-activation *in vitro* and *in vivo* (Klaiman *et al.*, 2009; Wang *et al.*, 2010). The three cleavage sites of CASP6 are TETD²³ after the pro-domain, and DVVD¹⁷⁹ and TEVD¹⁹³ in the intersubunit linker. Cleavage at either or both of the two intersubunit cleavage sites is sufficient for CASP6 activation (Klaiman *et al.*, 2009).

Recent studies have shown that CASP6 regulates axonal degeneration (Nikolaev *et al.*, 2009; Simon *et al.*, 2012). Moreover, there is increasing evidence that CASP6 plays crucial roles in neurodegenerative diseases, including

Huntington's disease and Alzheimer's disease (Graham *et al.*, 2006, 2010, 2011; Guo *et al.*, 2004; Albrecht *et al.*, 2007). Although the essentiality of CASP6 in pathogenesis is still debatable (Landles *et al.*, 2012), inhibition of CASP6 is widely considered to be a potential therapeutic method for these diseases.

The pro-domain, also known as the CARD (caspase-recruitment domain) or DED (death effector domain), is essential for the activation of initiator caspases (Yan & Shi, 2005; Pop & Salvesen, 2009). However, the pro-domains of effector caspases are considered to have no such function for two reasons. Firstly, compared with those of initiator caspases, the pro-domains of effector caspases are short (23–28 residues in length) and can hardly be defined as a 'domain'. Secondly, the pro-domains of initiator caspases mediate oligomeric activation *in vivo*, whereas effector caspases are stable dimers in both the zymogenic and the active states (Yan & Shi, 2005; Pop & Salvesen, 2009). At present, the function of effector caspase pro-domains is still unclear. For CASP6, the pro-domain inhibits its auto-activation *in vivo*, but not *in vitro* (Klaiman *et al.*, 2009); however, the pro-domain does not inhibit CASP3-induced activation of CASP6 (Wang *et al.*, 2010; Simon *et al.*, 2012) or CASP6 activity (Klaiman *et al.*, 2009; Vaidya *et al.*, 2011). In addition, the pro-domain of CASP6 is removed before cleavage at the intersubunit cleavage sites during auto-activation (Wang *et al.*, 2010).

Several crystal structures of CASP6 in different states or in complex with different inhibitors have been published (Wang *et al.*, 2010; Cao *et al.*, 2012; Baumgartner *et al.*, 2009; Vaidya *et al.*, 2011; Müller, Lamers, Ritchie, Park *et al.*, 2011; Müller, Lamers, Ritchie, Dominguez *et al.*, 2011; Velázquez-Delgado & Hardy, 2012; Stanger *et al.*, 2012; Heise *et al.*, 2012). Our previous study revealed a unique intramolecular self-activation mechanism of CASP6 (Wang *et al.*, 2010) and our subsequent study of the regulation of CASP6 phosphorylation further confirmed the self-activation mechanism and revealed the dual inhibitory mechanism of CASP6 phosphorylation (Cao *et al.*, 2012). In this study, we focused on the function of the pro-domain. We solved the crystal structure of the full-length catalytic inactive CASP6 zymogen, proCASP6H121A, and structural analyses and biochemical experiments disclosed the inhibitory mechanism of the pro-domain during the auto-activation of CASP6.

2. Materials and methods

2.1. Mutagenesis of CASP6

ProCASP6H121A and all of the other mutants were generated by overlapping PCR; the templates were wild-type CASP6 or previously generated mutants (Wang *et al.*, 2010; Cao *et al.*, 2012). All of the mutants used in this study are listed in Supplementary Table S1.¹

¹ Supporting information has been deposited in the IUCr electronic archive (Reference: MN5036).

Table 1

Data-collection statistics and crystallographic analysis of proCASP6H121A.

Values in parentheses are for the highest resolution shell.

Data collection	
Wavelength (Å)	0.9792
Space group	<i>I</i> ₄ 22
Unit-cell parameters (Å, °)	<i>a</i> = <i>b</i> = 158.06, <i>c</i> = 126.94, α = β = γ = 90
Resolution (Å)	50–2.7 (2.80–2.70)
<i>R</i> _{merge} [†] (%)	8.8 (56.6)
Mean <i>I</i> / σ (<i>I</i>)	20.5 (4.15)
Completeness (%)	97.6 (99.0)
Multiplicity	6.6
Refinement	
Resolution range (Å)	33–2.7
No. of reflections	21743
<i>R</i> _{work} / <i>R</i> _{free} [‡] (%)	18.1/23.0
Average <i>B</i> factor (Å ²)	48.8
R.m.s. deviation§	
Bond lengths (Å)	0.008
Bond angles (°)	1.117
Ramachandran plot, residues in (%)	
Most favoured region	94.82
Allowed region	5.18
Disallowed region	0

[†] $R_{\text{merge}} = \frac{\sum_{hkl} \sum_i |I_i(hkl) - \langle I(hkl) \rangle|}{\sum_{hkl} \sum_i I_i(hkl)}$. [‡] $R_{\text{work}} = \frac{\sum_{hkl} ||F_{\text{obs}}| - |F_{\text{calc}}||}{\sum_{hkl} |F_{\text{obs}}|}$. *R*_{free} values are calculated in the same way for a randomly selected 5% of the data that were excluded from the refinement. § Root-mean-square deviation from ideal/target geometries.

2.2. Protein preparation

All of the CASP6 mutants were expressed and purified as described previously (Cao *et al.*, 2012). The proCASP6H121A protein used for crystallization was purified by nickel-chelating column (HisTrap HP column, GE Healthcare, USA) and gel-filtration (120 ml Superdex 75, GE Healthcare) chromatography, and the other CASP6 mutants used for biochemical analysis were purified by nickel-chelating column and desalting column (5 ml HiTrap Desalting column, GE Healthcare) chromatography.

2.3. Crystallization and data collection

Crystals of proCASP6H121A were grown using the sitting-drop vapour-diffusion method. Crystals were obtained by incubating 10 mg ml⁻¹ protein (in 20 mM Tris–HCl pH 7.5, 150 mM NaCl, 10 mM dithiothreitol) with 0.1 M MES pH 6.2, 0.1 M sodium phosphate monobasic (NaH₂PO₄), 0.1 M potassium phosphate monobasic (KH₂PO₄), 1.75 M sodium chloride at 293 K. Crystallization solution containing 20% glycerol was used as a cryoprotectant. The crystal was flash-cooled and maintained at 100 K using nitrogen gas during X-ray diffraction data collection. The diffraction data were collected on beamline BL17U at the SSRF (Shanghai Synchrotron Radiation Facility), Shanghai, People's Republic of China at a wavelength of 0.98 Å. The data were processed using *HKL*-2000 (Otwinowski & Minor, 1997). The crystals belonged to space group *I*₄22 and each asymmetric unit contained one proCASP6H121A dimer.

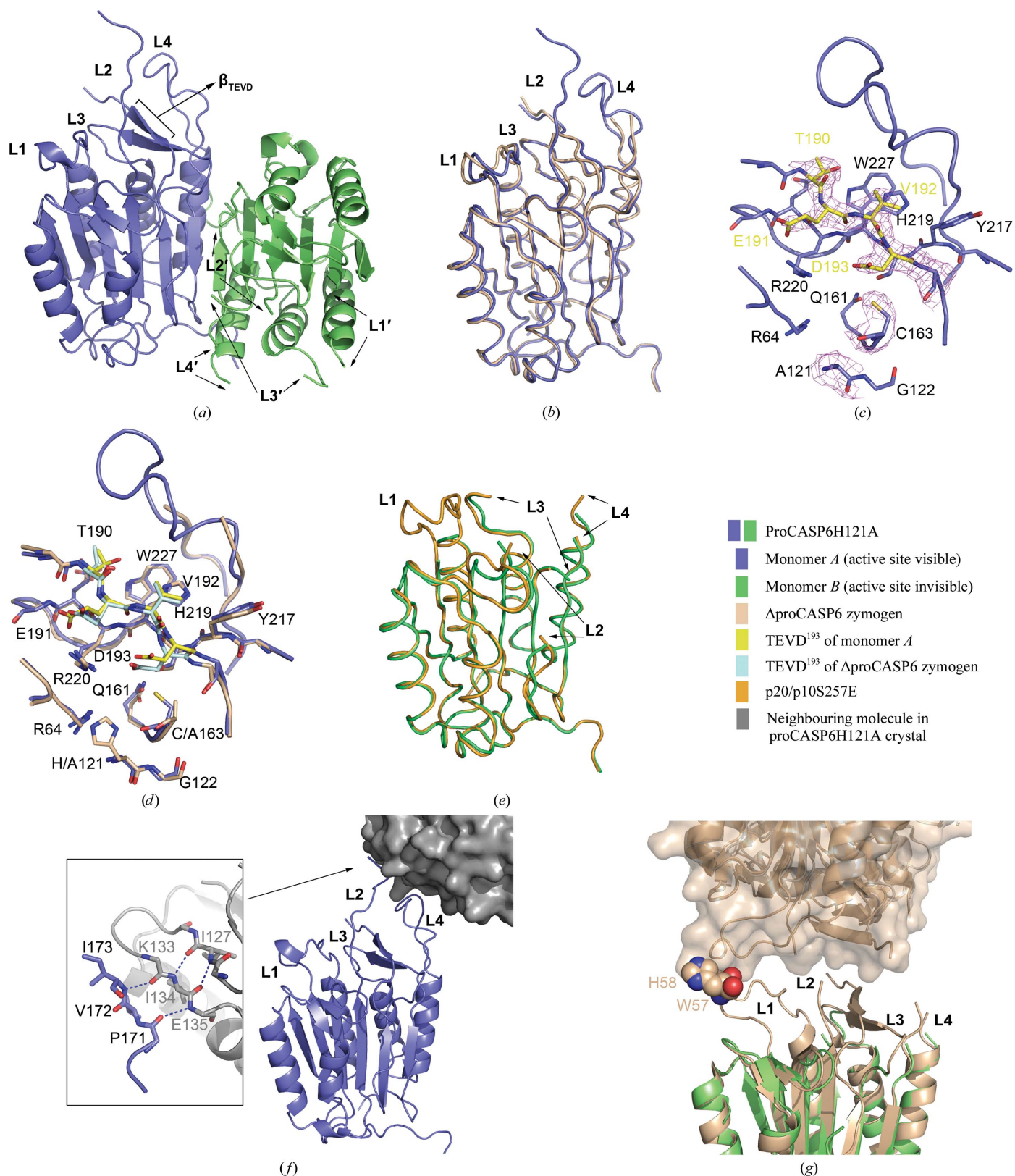


Figure 1

Structure of proCASP6H121A. (a) The overall structure of proCASP6H121A. (b) Structure overlay of monomer A of proCASP6H121A and the Δ proCASP6 zymogen. (c) Active site of monomer A. (d) Active-site overlay of monomer A of proCASP6H121A and the Δ proCASP6 zymogen. (e) Structure overlay of monomer B of proCASP6H121A and p20/p10S257E. (f) Interaction between monomer A and the neighbouring molecule in the proCASP6H121A crystal. (g) The clash between two well formed active sites of the Δ proCASP6 zymogen when superimposed on two symmetric B monomers of the proCASP6H121A crystal. The electron-density map ($2F_o - F_c$ maps) is shown at 1.0σ and was calculated by *phenix.refine*. Hydrogen bonds are shown as blue dashed lines.

2.4. Structure determination and refinement

The proCASP6H121A structure was determined by molecular-replacement calculations with *AutoMR* in *PHENIX* (Adams *et al.*, 2010) using the structure of the Δ proCASP6C163A dimer (PDB entry 3nr2; Wang *et al.*, 2010) as the search model. The model was built using *AutoBuild* in *PHENIX* (Adams *et al.*, 2010) and *Coot* (Emsley & Cowtan, 2004), and was further refined using *PHENIX* (Adams *et al.*, 2010). The PDB code for the structure of proCASP6H121A is 4iyf. The data-processing and refinement statistics are summarized in Table 1.

2.5. Cleavage assay of CASP6 variants

Purified CASP6 variants were diluted to $0.5 \mu\text{g } \mu\text{l}^{-1}$ ($\sim 16.7 \mu\text{M}$) and incubated with $5 \text{ ng } \mu\text{l}^{-1}$ ($\sim 0.167 \mu\text{M}$) wild-type CASP6 in the assay buffer (20 mM HEPES pH 7.4, 50 mM NaCl, 2 mM EDTA, 0.1% CHAPS, 5 mM DTT) for 30 min. Samples were analyzed by 15% SDS-PAGE.

2.6. Auto-activation assays of CASP6 variants

Auto-activation assays were performed as described previously (Cao *et al.*, 2012). Purified CASP6 variants were diluted to $0.2 \mu\text{g } \mu\text{l}^{-1}$ ($\sim 6.7 \mu\text{M}$) in the assay buffer containing $2 \mu\text{g } \mu\text{l}^{-1}$ ($\sim 30 \mu\text{M}$) bovine serum albumin (BSA) and were incubated at 310 K for 14 h. Samples were separated by 15% SDS-PAGE, transferred to Immobilon-P polyvinylidene fluoride (PVDF) membranes (Millipore, USA), probed with a 1:40 000 dilution of a rabbit anti-CASP6 serum and a 1:5000 dilution of secondary anti-rabbit IgG-HRP (MBL, USA) and detected with Metal Enhanced DAB Substrate Kit (Thermo Scientific, USA).

2.7. Enzyme-activity assays of active CASP6 with different substrates

The fluorogenic peptides Ac-Thr-Glu-Val-Asp-7-amino-4-trifluoromethyl coumarin (Ac-TEVD-AFC), Ac-Thr-Glu-Thr-Asp-amino-4-trifluoromethyl coumarin (Ac-TETD-AFC) and Ac-Met-Glu-Asn-Ala-Thr-Glu-Thr-Asp-amino-4-trifluoromethyl coumarin (Ac-MENATETD-AFC) were obtained from Hangzhou AngTai Biotechnology Co., People's Republic of China. The assays were performed in a 96-well plate and each well contained 50 ng purified wild-type CASP6 ($\sim 16.7 \text{ nM}$) and 500 ng BSA ($\sim 300 \text{ nM}$) in 100 μl assay buffer with 50 μM fluorogenic peptide. The activities were measured using an Infinite M200 multimode microplate reader (TECAN) with wavelengths of 400 nm for excitation and 505 nm for emission. The results were read at intervals of 1 min for up to 30 min. Fluorescence units were converted to the amount of released AFC based on a standard curve of 0–20 μM free AFC. Cleavage rates were calculated from the linear phase of the assays.

3. Results

3.1. Crystal structure of proCASP6H121A

To prevent self-activation and to obtain homogenous full-length CASP6 zymogen, the catalytic residues Cys163 or His121 were mutated to alanine. Both of the resulting mutants, proCASP6C163A and proCASP6H121A, were purified as stable homogeneous full-length proteins and were used for crystal screening. Visible crystals were only observed for proCASP6H121A. The structure of proCASP6H121A was determined to 2.7 Å resolution and refined to R_{work} and R_{free} values of 19.3 and 23.8%, respectively (Table 1).

The proCASP6H121A crystal contained a homodimer in the asymmetric unit and both monomers showed the typical caspase fold (Fig. 1*a*). This result agrees with prior biochemical and biophysical predictions (Kang *et al.*, 2002). The pro-domain was invisible in both monomers, although its existence was proved by SDS-PAGE of the proCASP6H121A crystal (Supplementary Fig. S1). The first visible residue at the N-terminus is Phe31 in both monomers. However, the active sites of the two monomers are in different conformations. One monomer has a well formed active site with all of the L1–L4 loops visible and will be referred to as monomer *A* in the following discussion. The other monomer has a disordered active site with all of the L1–L4 loops flexible without density, and will be referred to as monomer *B*.

Monomer *A* is almost identical to the Δ proCASP6 zymogen (PDB entry 3nr2; Wang *et al.*, 2010), with a root-mean-square deviation (r.m.s.d.) of 0.33 Å for all 214 aligned C $^{\alpha}$ atoms (Fig. 1*b*). The intersubunit cleavage site TEVD¹⁹³ in monomer *A* also binds in the active site as a β -strand (β_{TEVD}) with a well shaped density map (Fig. 1*c*). Both TEVD¹⁹³ and the residues forming the substrate-binding pockets overlap very well in monomer *A* and the Δ proCASP6 zymogen (Fig. 1*d*). The differences between these two structures are that monomer *A* of the proCASP6 zymogen shows an intact L4 loop and a longer visible L2 loop compared with the Δ proCASP6 zymogen. In monomer *A* only residues 174–186 of the L2 loop are flexible without electron density, whereas in the Δ proCASP6 zymogen residues 167–186 of the L2 loop and residues 262–270 of the L4 loop are flexible.

In contrast, in monomer *B* residues 53–66 of the L1 loop, residues 164–199 of the L2 loop, residues 214–221 of the L3 loop and residues 260–273 of the L4 loop are disordered without density. This monomer is almost identical to our previous solved p20/p10S257E structure (PDB entry 3v6m; Cao *et al.*, 2012), with an r.m.s.d. of 0.33 Å for 167 aligned C $^{\alpha}$ atoms (Fig. 1*e*). Most of the loops forming the active site were disordered in both structures. However, in p20/p10S257E the entire L1 loop is visible, whereas in monomer *B* of proCASP6H121A the L1 loop is also invisible.

To find out what causes the different conformations of the two monomers in proCASP6H121A, the interaction between each monomer and its neighbouring symmetry molecule in the proCASP6H121A crystal was investigated. In monomer *A*, the main-chain amino N atom of Ile173 and the main-chain ketonic O atom of Pro171 of the L2 loop form two hydrogen

bonds to the main-chain ketonic O atom of Lys133 and the main-chain amino N atom of Glu135 of the neighbouring molecule, respectively (Fig. 1*f*). The two hydrogen bonds stabilize the region from residues 167 to 173 of the L2 loop. Moreover, the L4 loop in monomer *A* is very close to the neighbouring molecule and this restriction may reduce the flexibility of the L4 loop and make the intact L4 loop visible in monomer *A*.

In contrast, in monomer *B* the crystal-packing environment is different. The neighbouring molecule of this monomer is on top of its active site and the active sites of two symmetric monomers face each other. Superimposing the Δ proCASP6 zymogen structure on both of the two symmetric monomers shows that the space between these two monomers does not allow two TEVD¹⁹³-bound active sites. If the two symmetric active sites both have TEVD¹⁹³ bound, the two β -hairpin structures of the L2 loops will clash with each other (Fig. 1*g*), and this β -hairpin structure is essential for TEVD¹⁹³ binding (Wang *et al.*, 2010). Meanwhile, our previous study shows that the L2, L3 and L4 loops are not well formed without substrate binding (Cao *et al.*, 2012). Furthermore, residues Tyr57 and His58 of the L1 loop also clash with each other in the two symmetric monomers if both of the L1 loops are well formed, which explains why the L1 loop of monomer *B* is also invisible.

The above structural analysis indicated that the different conformations of the two monomers in proCASP6H121A were caused by their packing environments. However, the question of which monomer represents the dominant conformation of the full-length zymogen in solution still needs to be further investigated. In most cases, invisibility suggests intrinsic flexibility; this may be stabilized by crystal packing, making the region visible, which means that monomer *B* may represent the solution conformation. Nevertheless, it is also possible that monomer *A* represents the solution conformation but that crystal packing restricts the formation of the TEVD¹⁹³-bound conformation in monomer *B*. The following biochemical experiments were performed to verify which monomer represents the conformation of the full-length zymogen in solution.

3.2. Cleavage assays suggest that TEVD¹⁹³ is still bound to the active site in the full-length CASP6 zymogen

In the TEVD¹⁹³-bound conformation, the TEVD¹⁹³ site is protected from intermolecular cleavage (Wang *et al.*, 2010). Only a slight amount of p20L appeared in the SDS-PAGE in the assay of proCASP6C163A cleaved by 1% active CASP6, whereas the proCASP6[C163A,R(64,220)E] mutant (the S1 pocket of this mutant was disrupted to release the TEVD¹⁹³ site) was completely cleaved by active CASP6 at the TEVD¹⁹³ site within 30 min (Wang *et al.*, 2010). A similar experiment was used to test which monomer of the proCASP6H121A structure represents the dominant conformation of proCASP6H121A in solution. H121A mutants with an uncleavable pro-domain or without the pro-domain, proCASP6(D23A,H121A) or Δ proCASP6H121A, respectively, were incubated with 1% active CASP6. For both proCASP6(D23A,H121A) and Δ proCASP6H121A only a small amount of pro-p20L or p20L appeared after incubation with active CASP6 for 30 min (Figs. 2*a* and 2*b*). These results indicated that both proCASP6(D23A,H121A) and Δ proCASP6H121A had a well formed TEVD¹⁹³-bound conformation in solution and further suggested that the existence of the pro-domain did not change or disturb the active-site conformation observed in the Δ proCASP6 zymogen (Wang *et al.*, 2010). Moreover, in combination with the crystal-packing analysis, these results suggested that in the proCASP6H121A structure monomer *A* represented the dominant conformation of full-length CASP6 in solution and the conformation of monomer *B* was caused by crystal packing.

3.3. The pro-domain inhibited the intramolecular cleavage of CASP6 at the TEVD¹⁹³ site

Klaiman and coworkers reported that the pro-domain inhibited CASP6 auto-activation *in vivo* but not *in vitro* (Klaiman *et al.*, 2009). One potential mechanism was pro-domain-inhibited CASP6 intramolecular self-cleavage. Our previous study suggested that CASP6 auto-activation was initiated by intramolecular cleavage (Wang *et al.*, 2010), but that intermolecular cleavage also contributed to CASP6 auto-activation at high protein concentrations (as discussed in detail in §4). In order to determine the influence of the pro-domain on intramolecular cleavage, a method is needed to distinguish intramolecular cleavage from intermolecular cleavage during *in vitro* CASP6 auto-activation. We found such a method of excluding intermolecular cleavage and focusing on intramolecular cleavage in the CASP6 phosphorylation study (Cao *et al.*, 2012). The

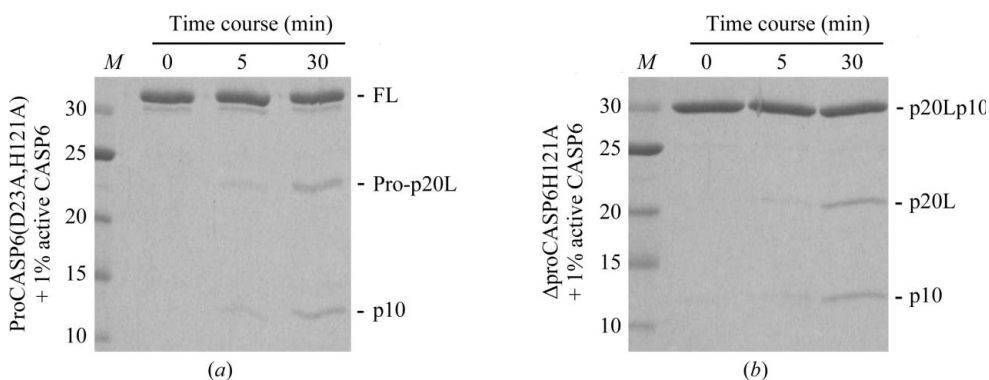


Figure 2 Cleavage assays of catalytic inactive CASP6 with or without pro-domain. Coomassie Blue-stained SDS-PAGE of (a) proCASP6(D23A,H121A) and (b) Δ proCASP6H121A incubated with 1% active CASP6 for 30 min. FL, full length; p20, large subunit; L, intersubunit linker; p10, small subunit.

phosphorylation of CASP6 at Ser257 inhibits CASP6 activation and activity by two different mechanisms (Cao *et al.*, 2012): it inhibits CASP6 activation by locking the protein in the TEVD¹⁹³-bound state through an interaction network and inhibits CASP6 activity by disrupting the formation of the active-site 'loop bundle' through steric hindrance. Five CASP6 mutants were found to regain the auto-activation ability but to have very low activity even after activation by CASP3 (Cao *et al.*, 2012) because these mutations break the interaction network but retain the steric hindrance. In other words, the auto-activation of these five mutants was only mediated by intramolecular cleavage. The five mutants were ΔproCASP6(S257E,Y217A), ΔproCASP6(S257E,K272A), ΔproCASP6(S257E,K273A), ΔproCASP6S257Q and ΔproCASP6S257K. The ΔproCASP6(S257E,K273A) and ΔproCASP6S257K mutants were chosen for the following auto-activation assay because the other three mutations introduced an extra interaction between the 257 site and the neighbouring 273 site [a salt bridge in ΔproCASP6(S257E,Y217A) and ΔproCASP6(S257E,K272A) and a hydrogen bond in ΔproCASP6S257Q] according to the structure analysis and these interactions do not exist in either the ΔproCASP6 zymogen or the active-site-visible monomer of full-length CASP6 structures.

The auto-activation abilities of the ΔproCASP6-(S257E,K273A), proCASP6(D23A,S257E,K273A), ΔproCASP6S257K and proCASP6(D23A,S257K) mutants were tested. The positive controls, ΔproCASP6(S257E,K273A) and ΔproCASP6S257K, underwent auto-activation during incubation, whereas the mutants with an uncleavable pro-domain, proCASP6(D23A,S257E,K273A) and proCASP6-(D23A,S257K), did not auto-activate: no pro-p20L band appeared after 14 h of incubation (Fig. 3). These results indicated that the pro-domain inhibited the intramolecular cleavage of CASP6.

3.4. The pro-domain cleavage site TETD²³ was cleaved prior to the cleavage of the intersubunit site TEVD¹⁹³ during intermolecular cleavage by active CASP6

Arg64 and Arg220 forming the S1 pocket were mutated to glutamate (this will be referred to as the RE mutation) to exclude TEVD¹⁹³ from the active site and make it accessible for intermolecular cleavage (Wang *et al.*, 2010). The pro-domain site, TETD²³, was cleaved before TEVD¹⁹³ even when both sites were accessible. A band corresponding to p20Lp10

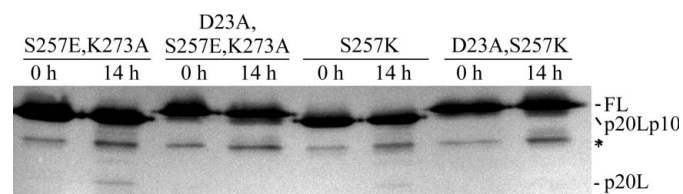


Figure 3 Auto-activation assay of CASP6 with or without pro-domain analyzed by Western blotting. The bands labelled with asterisks are a contaminating bacterial protein. FL, full length; p20, large subunit; L, intersubunit linker; p10, small subunit.

(representing TETD²³ prior to cleavage) appeared but no band corresponding to pro-p20L (representing TEVD¹⁹³ prior to cleavage) appeared on SDS-PAGE (Fig. 4a). This result suggested that the cleavage priority of the TETD²³ site was not owing to inaccessibility of the TEVD¹⁹³ site.

Talanian and coworkers reported that TETD and TEVD were both good substrates for CASP6 (Talanian *et al.*, 1997),

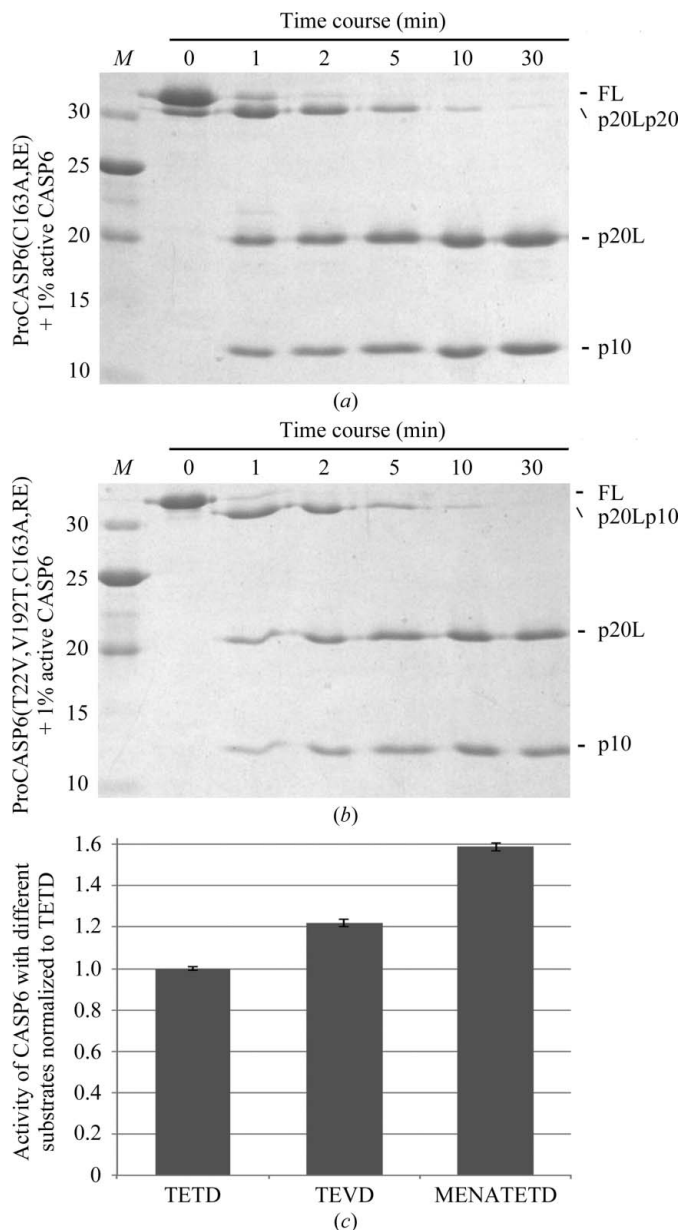


Figure 4 The priority of the TETD²³ site over the TEVD¹⁹³ site during intermolecular cleavage was not caused by the primary sequence. (a, b) Coomassie Blue-stained SDS-PAGE of (a) proCASP6(C163A,RE) and (b) proCASP6(T22V,V192T,C163A,RE) incubated with 1% active CASP6 for 30 min. (c) Activity assay of active CASP6 with different substrates. The concentration of the substrates was 50 μM and the concentration of active CASP6 was about 16.7 nM. The activities were normalized to the substrate Ac-TETD-AFC. Assays were performed in triplicate and error bars represent standard deviations. RE, R(64,220)E; FL, full length; p20, large subunit; L, intersubunit linker; p10, small subunit.

so the sequence itself should not make much difference to the cleavage priority. In addition, caspases prefer a small and uncharged residue after the P1 aspartate (also known as P1'; Timmer & Salvesen, 2007), but the P1' residues of the TETD²³ and TEVD¹⁹³ sites are both alanine, indicating that the P1'

residue does not cause the cleavage priority of the TETD²³ site either. To further investigate the reason for the cleavage priority, the two cleavage sites were exchanged and the resulting mutant, proCASP6(T22V,V192T,C163A,RE), was cleaved by active CASP6. In the cleavage assay, proCASP6

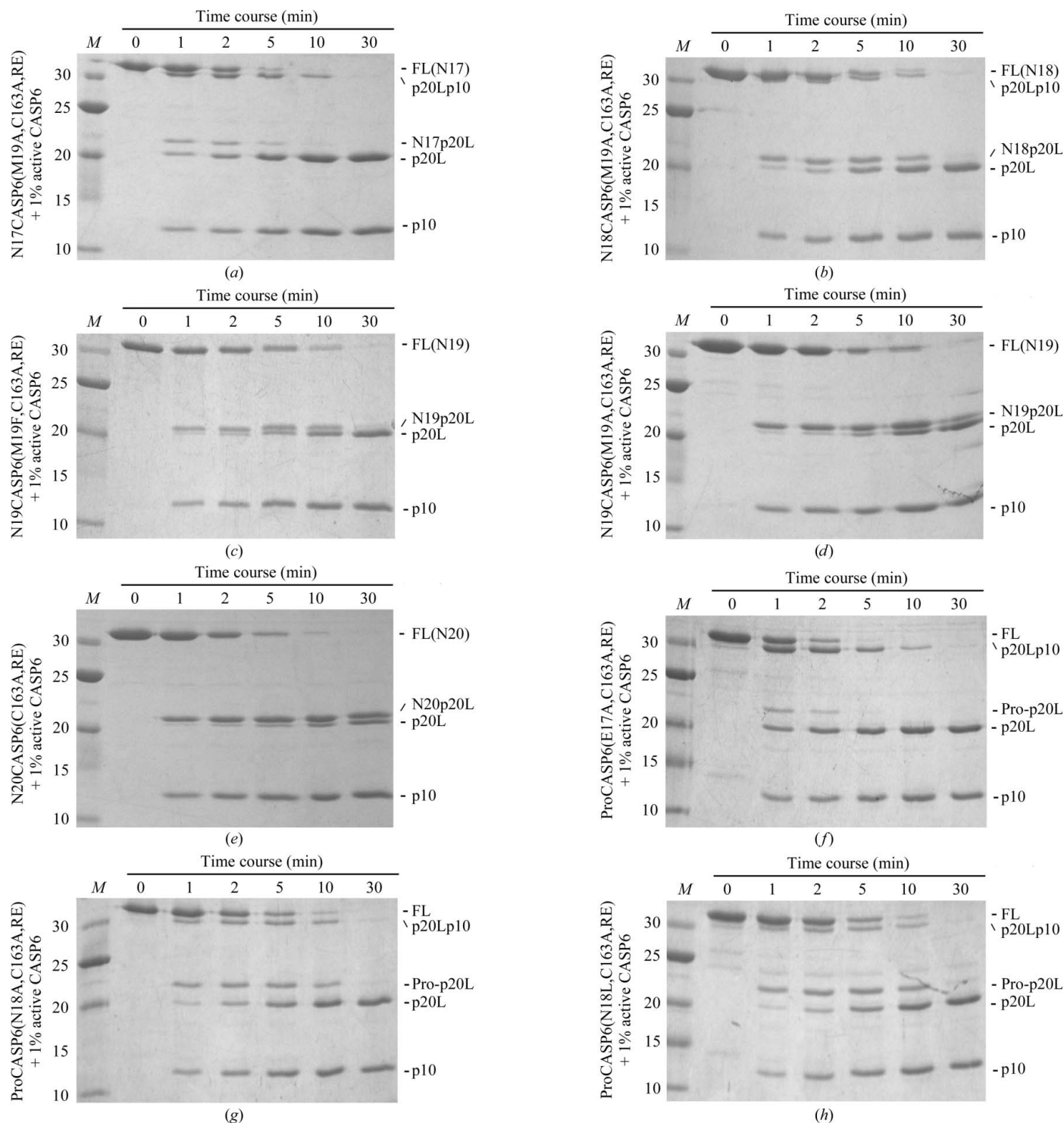


Figure 5 Cleavage assays of CASP6 pro-domain-related variants with the RE mutation. Coomassie Blue-stained SDS-PAGE of (a) N17CASP6(M19A, C163A,RE), (b) N18CASP6(M19A,C163A,RE), (c) N19CASP6(M19F,C163A,RE), (d) N19CASP6(M19A,C163A,RE), (e) N20CASP6(C163A,RE), (f) proCASP6(E17A,C163A,RE), (g) proCASP6(N18A,C163A,RE) and (h) proCASP6(N18L,C163A,RE) incubated with 1% active CASP6 for 30 min. RE, R(64,220)E; FL, full length; p20, large subunit; L, intersubunit linker; p10, small subunit.

(T22V,V192T,C163A,RE) showed a similar cleavage pattern to proCASP6(C163A,RE) (Fig. 4b). Furthermore, activity assays showed that the active CASP6 had a similar activity towards Ac-TETD-AFC and Ac-TEVD-AFC (Fig. 4c), and that Ac-TEVD-AFC was even a better substrate than Ac-TETD-AFC for CASP6. Both cleavage assays and activity assays suggested that the priority of the TETD²³ site over the TEVD¹⁹³ site during intermolecular cleavage was not caused by the sequence difference.

To investigate whether the N-terminal sequence of the TETD²³ site has any influence on the cleavage priority, one more peptide substrate was designed based on the following experiments, which showed that the priority still existed in the N17CASP6 truncation but not in the N20CASP6 truncation (discussed later; Figs. 5a and 5e). The peptide substrate Ac-MENATETD-AFC represents the pro-peptide sequence of the N17CASP6 mutant. CASP6 showed a relatively higher activity towards Ac-MENATETD-AFC than the two shorter peptides (Fig. 4c). However, the activity towards Ac-MENATETD-AFC was only about 1.3 times the activity towards Ac-TEVD-AFC and the activity difference alone was not sufficient to result in such a high cleavage priority of the TETD²³ site. Therefore, based on the experiments above, we propose that the cleavage priority of the TETD²³ site is caused by tertiary-structural factors rather than sequence differences.

3.5. Biochemical experiments showed the length of the pro-domain and the side chain of Asn18 were essential for TETD²³ site priority

Truncation experiments were performed to study whether the length of the pro-domain influences the TETD²³ site priority. The pro-domain was truncated from the N-terminus and the resulting truncations with the RE and C163A mutations were cleaved by active CASP6. The mutant with the N-terminal 16 residues deleted (starting from the 17th residue; referred to as N17CASP6), N17CASP6(M19A,C163A,RE), still showed cleavage priority of the TETD²³ site over the TEVD¹⁹³ site during intermolecular cleavage and very little pro-p20L appeared compared with the large amount of p20Lp10 on the SDS-PAGE gel (Fig. 5a). Met19 of the N17CASP6 mutant was mutated to alanine to exclude the second start point during expression and this mutation was verified to have no influence on the results (Supplementary Fig. S2). The N-terminal sequence of the resulting mutant N17CASP6(M19A,C163A,RE) was MENATETD. The first methionine was introduced as the translation initiator and this methionine was not removed during expression, because the first methionine is only digested during expression in *E. coli* when the following residue has a small side chain (Ben-Bassat *et al.*, 1987; Hirel *et al.*, 1989). Since the following truncations were truncated residue by residue, this N-terminal methionine needed to be considered. The truncation N18CASP6(M19A,C163A,RE), with an N-terminal sequence of MNATETD, showed almost equal amounts of p20Lp10 and pro-p20L in the cleavage assay (Fig. 5b), which suggested that the priority of TETD²³ had declined. The truncations

N19CASP6(M19F,C163A,RE), N19CASP6(M19A,C163A,RE) and N20CASP6(C163A,RE), the N-terminal sequences of which are MFTETD, ATETD and TETD, respectively, showed bands corresponding to pro-p20L but not to p20Lp10 on SDS-PAGE (Figs. 5c, 5d and 5e), which suggested that the priority of TETD²³ was totally removed. The above cleavage assays showed that truncations from MENATETD to MNATETD and from MNATETD to MFTETD made a great impact on the TETD²³ site priority. These results indicated that the length of the pro-domain influences the TETD²³ site priority, but it cannot be excluded that losing the side chain of Glu17 or Asn18 may also influence the priority.

To further investigate the influence of Glu17 and Asn18, the mutants proCASP6(E17A,C163A,RE) and proCASP6(N18A,C163A,RE) were generated and cleaved by active CASP6. The results showed that the E17A mutation had no influence on the TETD²³ site priority (Fig. 5f), whereas the mutation N18A decreased the TETD²³ site priority (Fig. 5g). These results indicated that the decline in TETD²³ site priority on truncation from MENATETD to MNATETD was caused by the loss of the Glu17 main chain (length difference) and further suggested that an eight-residue length was the minimum for the pro-domain to maintain the TETD²³ site priority during intermolecular cleavage. Besides the main-chain length, the side chain of Asn18 was also essential for the TETD²³ site priority. To study the function of Asn18 further, Asn18 was mutated to leucine. The resulting mutant proCASP6(N18L,C163A,RE) also showed a decreased TETD²³ site priority in the cleavage assay (Fig. 5h), which suggested that Asn18 does not maintain the TETD²³ site priority by its side-chain size. The hydrophilicity and the ability to form a hydrogen bond of the Asn18 side chain might be important for the TETD²³ site priority, but no definite conclusion can be made without structural information.

4. Discussion

The pro-domain inhibits the auto-activation of CASP6 *in vivo* but not *in vitro* (Klaiman *et al.*, 2009). In order to reveal the inhibitory mechanism of the pro-domain, we solved the crystal structure of the full-length CASP6 zymogen. Although the pro-domain was invisible in the structure, structure analysis combined with biochemical experiments still provided some important information about the function and the regulation mechanism of the CASP6 pro-domain. Firstly, structure analysis and cleavage assays indicated that the full-length CASP6 zymogen had the same TEVD¹⁹³-bound conformation as the ΔproCASP6 zymogen and further suggested that the pro-domain did not regulate CASP6 activity through active-site conformational changes. Secondly, the flexibility of the pro-domain also suggested that the pro-domain did not stably bind to a location on CASP6 to perform regulation. Based on the structure analysis and the biochemical results, we proposed a regulation mechanism in which the pro-domain inhibits CASP6 auto-activation by inhibiting intramolecular cleavage at the intersubunit cleavage site TEVD¹⁹³ and also by preventing this site from intermolecular cleavage at low

protein concentrations through 'suicide protection'. However, although less likely, another possibility that the invisibility of the pro-domain is caused by crystal packing cannot be excluded, which means that the pro-domain might be visible in other crystals in a different space group. Nevertheless, no structure of an effector pro-caspase with a visible pro-domain has been reported to date and the results presented in this study support the flexible conformation of the pro-domain represented by its natural state in solution (as further discussed below).

This study also extended our understanding of the CASP6 auto-activation mechanism. Since the first CASP6 structure was solved and the novel TEVD¹⁹³-bound conformation was first observed (Wang *et al.*, 2010), several CASP6 zymogen structures have been solved and they all show the same TEVD¹⁹³-bound conformation. These crystal structures belong to different crystal space groups, such as *P*₆₅₂₂ for the ΔproCASP6 zymogen (Wang *et al.*, 2010) and ΔproCASP6S257E (Cao *et al.*, 2012) (PDB entries 3nr2 and 3v6l, respectively); *C*2 for the CASP6 zymogen complex with allosteric peptides (Stanger *et al.*, 2012; PDB entry 4ejf); and *I*₄₂₂ for the full-length CASP6 zymogen. All of these structures in different space groups solved by different groups confirm that the TEVD¹⁹³-bound conformation truly exists.

Based on the TEVD¹⁹³-bound conformation and relevant biochemical assays, we revealed a unique intramolecular cleavage mechanism for CASP6 auto-activation (Wang *et al.*, 2010) and this mechanism agreed with our structure analysis, biochemical assays and MD simulations. However, this mechanism is still not fully accepted, because to date no direct evidence has been found to prove that the auto-activation of CASP6 is caused by intramolecular cleavage. The intermolecular cleavage also contributes to *in vitro* CASP6 auto-activation, which is the most important reason why direct evidence for intramolecular cleavage is difficult to find. The TEVD¹⁹³ site of the catalytically inactive CASP6 zymogen is hardly cleaved when incubated with 1% active CASP6 (Wang *et al.*, 2010), but when incubated with 10% active CASP6 the catalytic inactive CASP6 zymogen was processed within hours (Velázquez-Delgado & Hardy, 2012). These results suggest that the TEVD¹⁹³ site is flexible enough to move out of the active site randomly and be digested through intermolecular cleavage. During *in vitro* auto-activation, although no active CASP6 was previously added, the CASP6 zymogen itself has approximately 4% activity compared with activated CASP6 (Vaidya *et al.*, 2011), which can be simply counted as 4% active CASP6 incubated with 96% catalytically inactive CASP6. In this case, cleavage at TEVD¹⁹³ produces the fully active enzyme, which forms a positive-feedback cascade and speeds up the auto-activation. This hypothesis was confirmed by a concentration-dependence assay of the *in vitro* CASP6 auto-activation. The speed of CASP6 auto-activation was correlated with the CASP6 concentration (Supplementary Fig. S3), suggesting that CASP6 auto-activation was accelerated by intermolecular cleavage *in vitro*. However, the concentration of the CASP6 zymogen *in vivo* is probably too low for intermolecular cleavage: the endogenous concentration of CASP6

was 33 and 64 nM in HEK293T and Jurkat cells, respectively (Klaiman *et al.*, 2009); therefore, intramolecular cleavage is essential for *in vivo* auto-activation. In this study, auto-activation assays of the CASP6 mutants successfully excluded the influence of intermolecular cleavage and mimicked the *in vivo* auto-activation *in vitro*, and showed that the pro-domain inhibited intramolecular cleavage of CASP6. This result plus the fact that the pro-domain did not inhibit CASP6 auto-activation *in vitro* suggested that intermolecular cleavage itself was sufficient for CASP6 auto-activation when the concentration was high *in vitro*. In addition, the finding that the pro-domain inhibits CASP6 auto-activation *in vivo* (Klaiman *et al.*, 2009) confirms that intramolecular cleavage was essential to CASP6 auto-activation *in vivo*.

Besides inhibiting intramolecular self-cleavage at TEVD¹⁹³, the cleavage priority of the TETD²³ site over the TEVD¹⁹³ site during intermolecular self-cleavage makes the pro-domain act as a 'suicide protector' which also protects the TEVD¹⁹³ site from intermolecular self-cleavage. Because intermolecular self-cleavage will only occur when the TEVD¹⁹³ site moves out and meets another unoccupied active site, the rate-limiting step is meeting another molecule at low protein concentration. Therefore, although the TETD²³ site can only protect the TEVD¹⁹³ site once, this protection makes the chance of intermolecular cleavage at TEVD¹⁹³ much lower. In other words, this protection can slow down intermolecular self-cleavage and the lower the protein concentration is, the more effective it will be. In the *in vivo* condition, the concentration of CASP6 is very low and intermolecular self-cleavage at the TEVD¹⁹³ site can be effectively inhibited by the TETD²³ site-mediated protection.

The biochemical assays showed that the mechanism of this 'suicide protection' was not owing to sequence specificity but to tertiary-structural factors. However, because the pro-domain is flexible without density in the full-length CASP6 structure the exact mechanism of the TETD²³ site priority is unclear, but this study still provides some clues. One possibility is that the pro-domain is located on top of the TEVD¹⁹³ site and shields it against intermolecular cleavage, which explains why almost none of the TEVD¹⁹³ site was cleaved before the TETD²³ site and why the length of the pro-domain was essential to this prioritization. Additionally, the Asn18 residue might form hydrogen bonds to other residues near the TEVD¹⁹³ site to stabilize the location of the pro-domain. In this case, a flexible and unstructured pro-domain might even benefit its function, because its flexibility might provide a larger shielded area and an unstructured peptide could be a better substrate than a structured peptide. Based on the analysis, the invisible pro-domain in the full-length CASP6 structure is not an unexpected finding and it is more likely to represent the natural state of the full-length CASP6.

The full-length zymogen structure combined with our previous solved structures of the ΔproCASP6 zymogen (PDB entry 3nr2), an inhibitor-bound state (PDB entry 3od5) and two phosphorylated states (PDB entries 3v6l and 3v6m) reveal the whole picture of CASP6 auto-activation and regulation, including intramolecular self-activation, phosphorylation-

mediated inhibition and the regulatory function of the pro-domain. Because of the crucial roles of CASP6 in neurodegenerative diseases, these structural and biochemical studies provide clues and a necessary structural basis for controlling the activation and activity of CASP6 at different levels and through different methods, and provide important information for the potential pathogenesis of and new therapeutic inspiration for CASP6-related diseases.

We thank Drs Xiang-Yu Liu and Dong Xing and Mr Jian-Shi Jin for valuable discussions and thank Wen-Sheng Wei for providing the microplate reader. This work was supported by a grant from the National Basic Research Program of China (973 Program; grant No. 2011CB911103 to X-DS).

References

- Adams, P. D. *et al.* (2010). *Acta Cryst.* **D66**, 213–221.
- Albrecht, S., Bourdeau, M., Bennett, D., Mufson, E. J., Bhattacharjee, M. & LeBlanc, A. C. (2007). *Am. J. Pathol.* **170**, 1200–1209.
- Baumgartner, R., Meder, G., Briand, C., Decock, A., D'arcy, A., Hassiepen, U., Morse, R. & Renatus, M. (2009). *Biochem. J.* **423**, 429–439.
- Ben-Bassat, A., Bauer, K., Chang, S.-Y., Myambo, K., Boosman, A. & Chang, S. (1987). *J. Bacteriol.* **169**, 751–757.
- Boatright, K. M. & Salvesen, G. S. (2003). *Curr. Opin. Cell Biol.* **15**, 725–731.
- Cao, Q., Wang, X.-J., Liu, C.-W., Liu, D.-F., Li, L.-F., Gao, Y.-Q. & Su, X.-D. (2012). *J. Biol. Chem.* **287**, 15371–15379.
- Emsley, P. & Cowtan, K. (2004). *Acta Cryst.* **D60**, 2126–2132.
- Graham, R. K., Deng, Y., Carroll, J., Vaid, K., Cowan, C., Pouladi, M. A., Metzler, M., Bissada, N., Wang, L., Faull, R. L. M., Gray, M., Yang, X. W., Raymond, L. A. & Hayden, M. R. (2010). *J. Neurosci.* **30**, 15019–15029.
- Graham, R. K. *et al.* (2006). *Cell*, **125**, 1179–1191.
- Graham, R. K., Ehrnhoefer, D. E. & Hayden, M. R. (2011). *Trends Neurosci.* **34**, 646–656.
- Guo, H., Albrecht, S., Bourdeau, M., Petzke, T., Bergeron, C. & LeBlanc, A. C. (2004). *Am. J. Pathol.* **165**, 523–531.
- Heise, C. E. *et al.* (2012). *PLoS One*, **7**, e50864.
- Hirel, P. H., Schmitter, M. J., Dessen, P., Fayat, G. & Blanquet, S. (1989). *Proc. Natl Acad. Sci. USA*, **86**, 8247–8251.
- Kang, B. H., Ko, E., Kwon, O.-K. & Choi, K. Y. (2002). *Biochem. J.* **364**, 629–634.
- Klaiman, G., Champagne, N. & LeBlanc, A. C. (2009). *Biochim. Biophys. Acta*, **1793**, 592–601.
- Landles, C., Weiss, A., Franklin, S., Howland, D. & Bates, G. (2012). *PLoS Curr.* **4**, e4fd085bfc9973.
- Müller, I., Lamers, M. B., Ritchie, A. J., Dominguez, C., Munoz-Sanjuan, I. & Kiselyov, A. (2011). *Bioorg. Med. Chem. Lett.* **21**, 5244–5247.
- Müller, I., Lamers, M. B., Ritchie, A. J., Park, H., Dominguez, C., Munoz-Sanjuan, I., Maillard, M. & Kiselyov, A. (2011). *J. Mol. Biol.* **410**, 307–315.
- Nikolaev, A., McLaughlin, T., O'Leary, D. D. & Tessier-Lavigne, M. (2009). *Nature (London)*, **457**, 981–989.
- Otwinowski, Z. & Minor, W. (1997). *Methods Enzymol.* **276**, 307–326.
- Pop, C. & Salvesen, G. S. (2009). *J. Biol. Chem.* **284**, 21777–21781.
- Simon, D. J., Weimer, R. M., McLaughlin, T., Kallop, D., Stanger, K., Yang, J., O'Leary, D. D. M., Hannoush, R. N. & Tessier-Lavigne, M. (2012). *J. Neurosci.* **32**, 17540–17553.
- Slee, E. A., Harte, M. T., Kluck, R. M., Wolf, B. B., Casiano, C. A., Newmeyer, D. D., Wang, H.-G., Reed, J. C., Nicholson, D. W., Alnemri, E. S., Green, D. R. & Martin, S. J. (1999). *J. Cell Biol.* **144**, 281–292.
- Stanger, K., Steffek, M., Zhou, L., Pozniak, C. D., Quan, C., Franke, Y., Tom, J., Tam, C., Krylova, I., Elliott, J. M., Lewcock, J. W., Zhang, Y., Murray, J. & Hannoush, R. N. (2012). *Nature Chem. Biol.* **8**, 655–660.
- Talanian, R. V., Quinlan, C., Trautz, S., Hackett, M. C., Mankovich, J. A., Banach, D., Ghayur, T., Brady, K. D. & Wong, W. W. (1997). *J. Biol. Chem.* **272**, 9677–9682.
- Timmer, J. C. & Salvesen, G. S. (2007). *Cell Death Differ.* **14**, 66–72.
- Vaidya, S., Velázquez-Delgado, E. M., Abbruzzese, G. & Hardy, J. A. (2011). *J. Mol. Biol.* **406**, 75–91.
- Velázquez-Delgado, E. M. & Hardy, J. A. (2012). *Structure*, **20**, 742–751.
- Wang, X.-J., Cao, Q., Liu, X., Wang, K.-T., Mi, W., Zhang, Y., Li, L.-F., LeBlanc, A. C. & Su, X.-D. (2010). *EMBO Rep.* **11**, 841–847.
- Yan, N. & Shi, Y. (2005). *Annu. Rev. Cell Dev. Biol.* **21**, 35–56.